Supramolecular charge transfer adducts of rare earth 3,5-dinitrobenzoates and diaminodurene: a new approach to increasing spin density in lanthanide complexes

Pavel S. Koroteev[1]*, Andrey B. Ilyukhin[1], Vadim V. Minin[1], Zhanna V. Dobrokhotova[1], Natalia N. Breslavskaya[1], Elena N. Timokhina[2], Elena A. Ugolkova[1], Amgalanbaatar Baldansuren[3,4], Floriana Tuna[3], Nikolay N. Efimov[1]

[1]*N.S. Kurnakov Institute of General and Inorganic Chemistry, Russian Academy of Sciences, Leninsky prosp. 31, 119991 Moscow, GSP-1, Russian Federation*

[2]*N. M. Emanuel Institute of Biochemical Physics, Russian Academy of Sciences, 4 Kosygina str., 119334 Moscow, Russian Federation*

[3] *EPSRC National EPR Facility and Service, Department of Chemistry and Photon Science Institute, University of Manchester, Manchester, M13 9PL, UK*

[4]*Department of Chemistry and Chemical Biology, Rensselaer Polytechnic Institute, Troy, NY 12180, USA*

SUPPLEMENTARY MATERIALS

Table S1. Crystal data and structure refinement for compounds **1-7**.

Identification code	**1**	**2**	**3**	**4**	**5**	**6**	**7**
Empirical formula	$C_{90}H_{106}N_{20}O_{40}S_4Sm_2$	$C_{90}H_{106}Gd_2N_{20}O_{40}S_4$	$C_{90}H_{106}N_{20}O_{40}S_4Tb_2$	$C_{90}H_{106}Dy_2N_{20}O_{40}S_4$	$C_{90}H_{106}Ho_2N_{20}O_{40}S_4$	$C_{90}H_{106}Er_2N_{20}O_{40}S_4$	$C_{90}H_{106}N_{20}O_{40}S_4Y_2$
Formula weight	2536.88	2550.68	2554.02	2561.18	2566.04	2570.70	2414.00
Temperature, K	173(2)	120(2)	173(2)	173(2)	173(2)	153(2)	120(2)
Wavelength, Å	0.71073	0.71073	0.71073	0.71073	0.71073	0.71073	0.71073
Crystal system	Monoclinic	Monoclinic	Monoclinic	Monoclinic	Monoclinic	Monoclinic	Monoclinic
Space group	$P2_1/n$	$P2_1/n$	$P2_1/n$	$P2_1/n$	$P2_1/n$	$P2_1/n$	$P2_1/n$
a, Å	13.6528(3)	13.6059(6)	13.6262(5)	13.6161(3)	13.6054(5)	13.5955(6)	13.5906(3)
b, Å	25.0658(5)	24.9355(10)	25.0293(8)	25.0372(5)	25.0164(9)	25.0342(11)	24.9418(5)
c, Å	15.3632(3)	15.2921(6)	15.3375(5)	15.3325(3)	15.3117(6)	15.3116(7)	15.2728(3)
β, °	98.3460(10)	98.3190(10)	98.1270(10)	98.1250(10)	98.1120(10)	97.9640(10)	98.1120(10)
Volume, $Å^3$	5201.89(19)	5133.6(4)	5178.4(3)	5174.52(18)	5159.3(3)	5161.1(4)	5125.28(18)
Z	2	2	2	2	2	2	2
D (calc), Mg/m^3	1.620	1.650	1.638	1.644	1.652	1.654	1.564
μ, mm^{-1}	1.296	1.462	1.534	1.613	1.703	1.795	1.308
F(000)	2588	2596	2600	2604	2608	2612	2496
Crystal size, mm	0.32 x 0.24 x 0.2	0.24 x 0.18 x 0.16	0.3 x 0.24 x 0.2	0.3 x 0.26 x 0.2	0.3 x 0.26 x 0.2	0.35 x 0.3 x 0.2	0.28 x 0.24 x 0.2
θ range, °	2.305, 31.056	2.314, 26.424	2.305, 31.540	2.306, 32.029	2.308, 31.554	2.306, 31.528	2.049, 28.315
Index ranges	-19<=h<=19	-16<=h<=16	-20<=h<=19	-19<=h<=19	-19<=h<=19	-19<=h<=19	-18<=h<=17
	-27<=k<=36	-31<=k<=30	-36<=k<=36	-35<=k<=36	-36<=k<=36	-36<=k<=36	-33<=k<=33
	-22<=l<=22	-19<=l<=18	-22<=l<=22	-22<=l<=21	-21<=l<=21	-22<=l<=21	-20<=l<=20
Reflections collected	49055	54280	74116	74742	72766	73754	57606
Independent reflections, Rint	16113, 0.0316	10506, 0.0604	16613, 0.0339	16588, 0.0377	16481, 0.0373	16536, 0.0324	12745, 0.0599
Completeness to θ = 25.242°	99.9 %	99.9 %	99.9 %	99.9 %	99.9 %	99.9 %	100.0 %
Absorption correction	Semi-empirical from equivalents	Semi-empirical from equivalents	Semi-empirical from equivalents	Semi-empirical from equivalents	Semi-empirical from equivalents	Semi-empirical from equivalents	Semi-empirical from equivalents
Max,. min. transmission	0.7462, 0.594	0.7454, 0.6486	0.7462, 0.5587	0.7463, 0.6097	0.7462, 0.585	0.7462, 0.6174	0.7457, 0.5937
Refinement method	Full-matrix least-squares on F^2	Full-matrix least-squares on F^2	Full-matrix least-squares on F^2	Full-matrix least-squares on F^2	Full-matrix least-squares on F^2	Full-matrix least-squares on F^2	Full-matrix least-squares on F^2
Data / restraints / parameters	16113 / 0 / 718	10506 / 0 / 719	16613 / 0 / 719	16588 / 0 / 716	16481 / 0 / 718	16536 / 0 / 718	12745 / 0 / 719
Goodness-of-fit	1.037	1.084	1.065	1.044	1.052	1.094	1.055
R1, wR2 [I>2sigma(I)]	0.0320, 0.0769	0.0400, 0.0885	0.0310, 0.0790	0.0320, 0.0790	0.0332, 0.0798	0.0315, 0.0813	0.0487, 0.1245
R1, wR2 (all data)	0.0428, 0.0818	0.0608, 0.0972	0.0410, 0.0841	0.0436, 0.0847	0.0465, 0.0863	0.0419, 0.0865	0.0826, 0.1398
Largest diff. peak and hole, $e.Å^{-3}$	1.310, -0.546	1.674, -0.760	1.064, -0.683	1.148, -0.648	1.319, -0.742	1.369, -0.830	1.208, -0.794

Table S2. Bond lengths Ln-O for **1-7**, Å.

Identification code	**1**	**2**	**3**	**4**	**5**	**6**	**7**
Ln	Sm	Gd	Tb	Dy	Ho	Er	Y
Ln(1)-O(8)#1	2.3626(15)	2.330(3)	2.3196(16)	2.3079(17)	2.2934(18)	2.2788(17)	2.294(2)
Ln(1)-O(1)	2.3696(15)	2.346(3)	2.3338(16)	2.3221(17)	2.3107(18)	2.2995(18)	2.310(2)
Ln(1)-O(19)	2.3709(16)	2.348(3)	2.3342(17)	2.3198(17)	2.3113(18)	2.2993(19)	2.300(2)
Ln(1)-O(2)#1	2.3819(15)	2.347(3)	2.3383(16)	2.3266(17)	2.3147(17)	2.3001(17)	2.311(2)
Ln(1)-O(7)	2.4155(15)	2.387(3)	2.3793(16)	2.3675(16)	2.3546(17)	2.3437(17)	2.354(2)
Ln(1)-O(13)	2.4417(15)	2.410(3)	2.3998(16)	2.3876(17)	2.3788(18)	2.3685(17)	2.375(2)
Ln(1)-O(20)	2.4603(15)	2.434(3)	2.4253(17)	2.4157(18)	2.4041(18)	2.3925(19)	2.404(2)
Ln(1)-O(14)	2.5540(17)	2.531(3)	2.5214(18)	2.5086(18)	2.4938(19)	2.487(2)	2.489(2)
Ln(1)…Ln(1)#1	4.5680(2)	4.5383(4)	4.5137(2)	4.5049(2)	4.4891(2)	4.4755(2)	4.4978(5)

Symmetry transformations used to generate equivalent atoms:

#1 -x, -y, -z

Table S3. Hydrogen bonds for compound **3** (Å and °).

D-H...A	d(D-H)	d(H...A)	d(D...A)	<(DHA)
N(7)-H(1)...O(7)	0.90	2.38	3.154(3)	144
N(7)-H(2)...O(13)	0.90	2.45	3.111(3)	131
N(8)-H(3)...O(17)#1	0.90	2.48	3.336(5)	159
N(8)-H(4)...O(15)	0.90	2.58	3.441(5)	161
N(9)-H(5)...O(3)#1	0.90	2.36	3.233(4)	164
N(9)-H(6)...O(12)#2	0.90	2.34	3.210(4)	162
N(10)-H(7)...N(6)	0.90	2.52	3.296(4)	145
N(10)-H(8)...S(2)#3	0.90	2.84	3.711(3)	163

Symmetry transformations used to generate equivalent atoms:

#1 x+1/2, -y+1/2, z+1/2; #2 x, y, z+1; #3 -x+1/2, y+1/2, -z+1/2

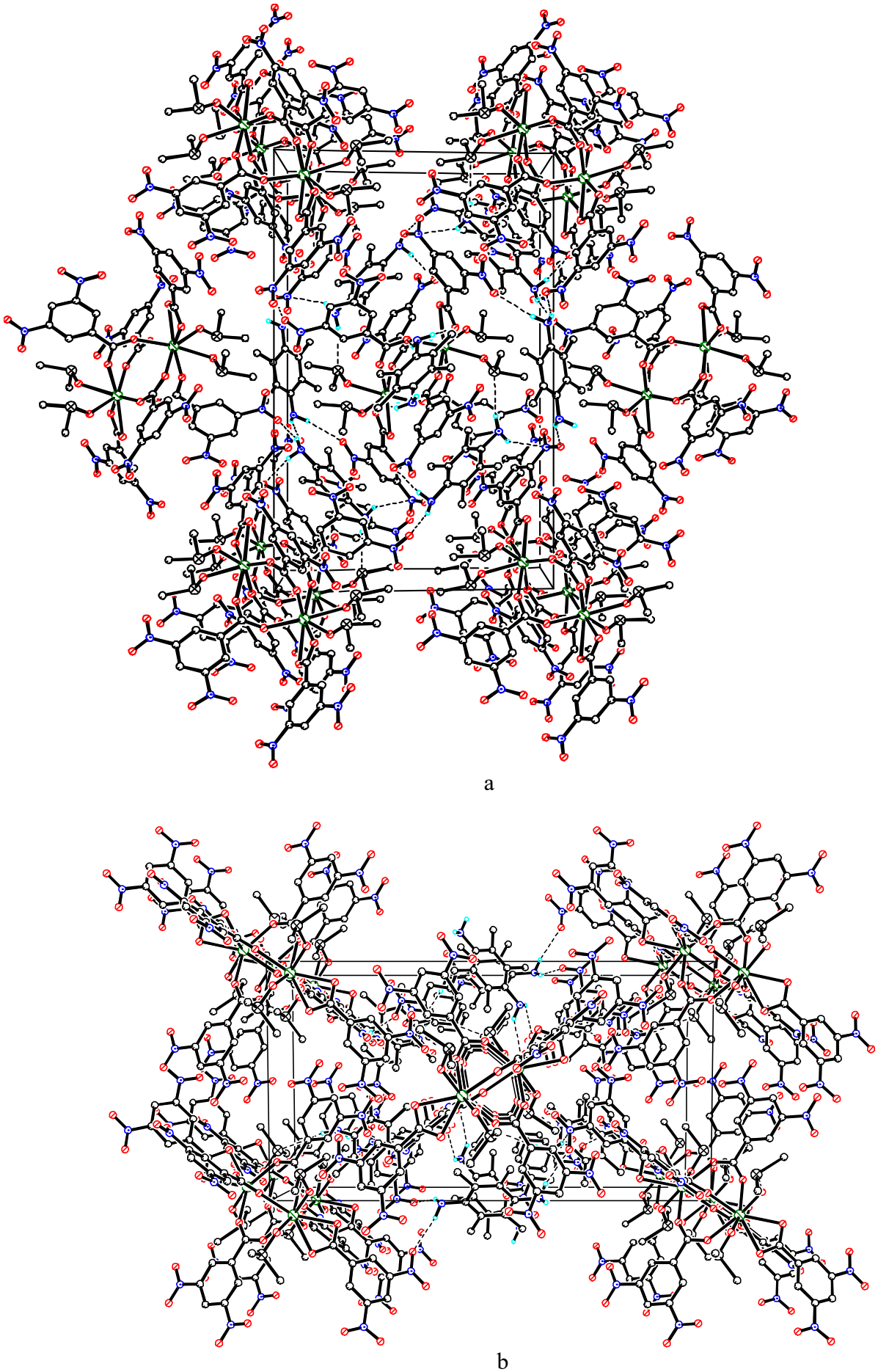

Fig. S1. Projection of the structure **3** along the axes x (a), z (b). Only the H atoms of NH_2 groups are shown for clarity.

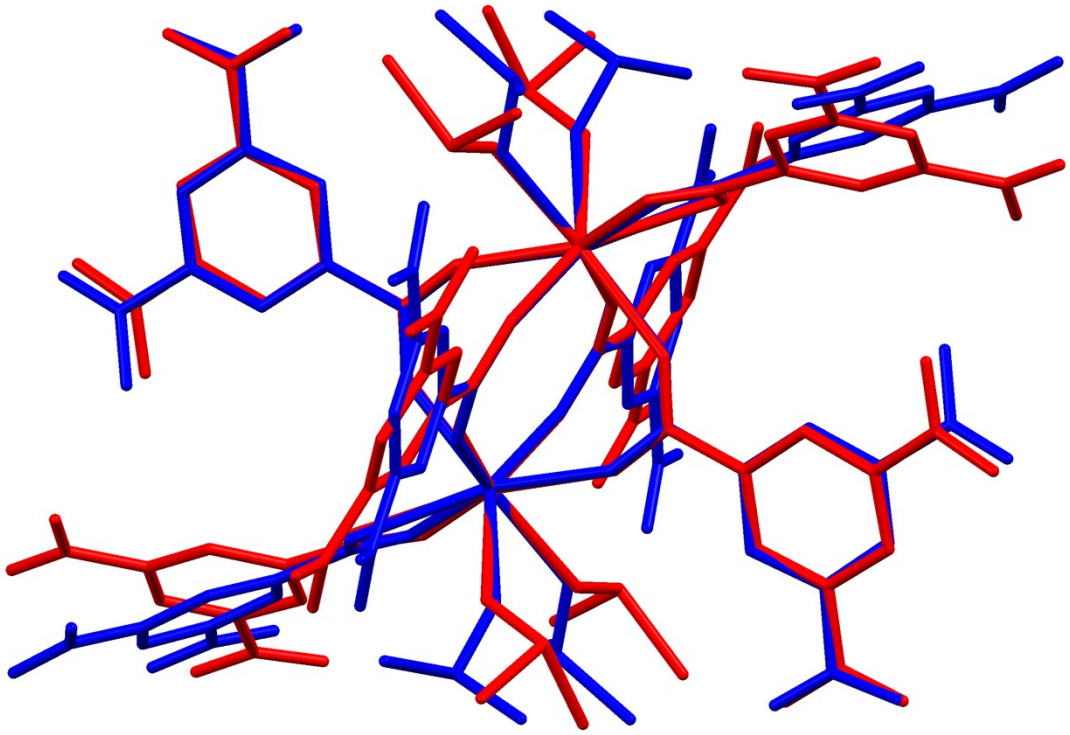

a

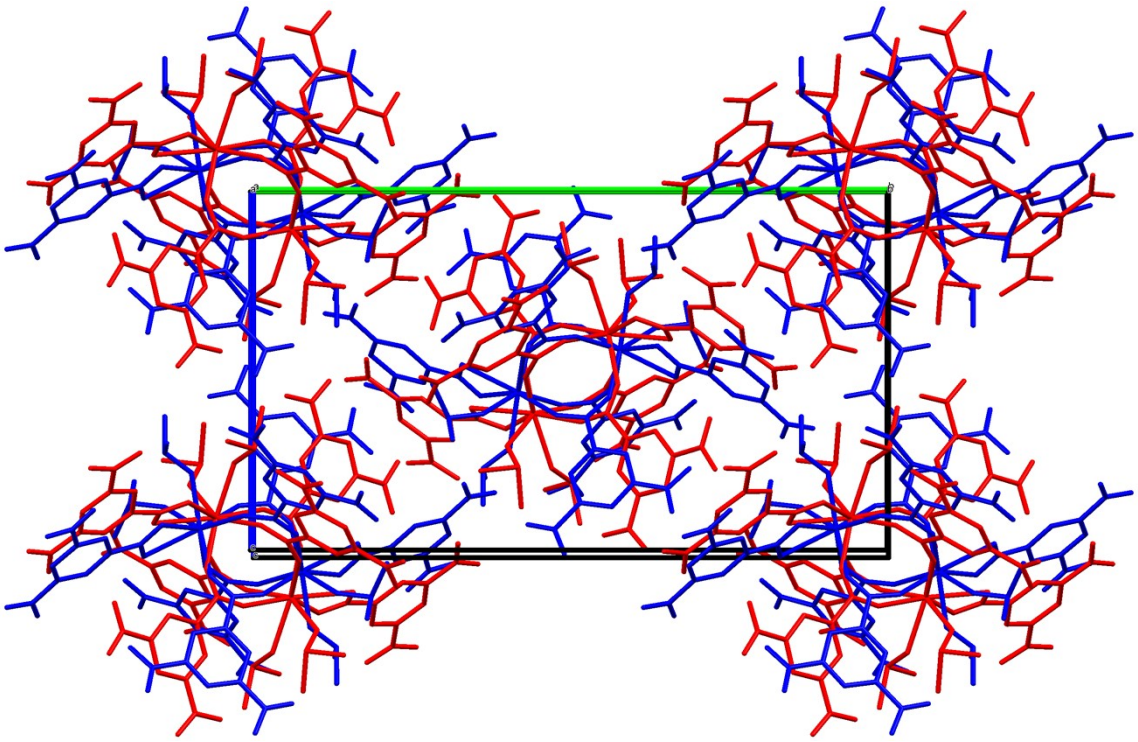

b

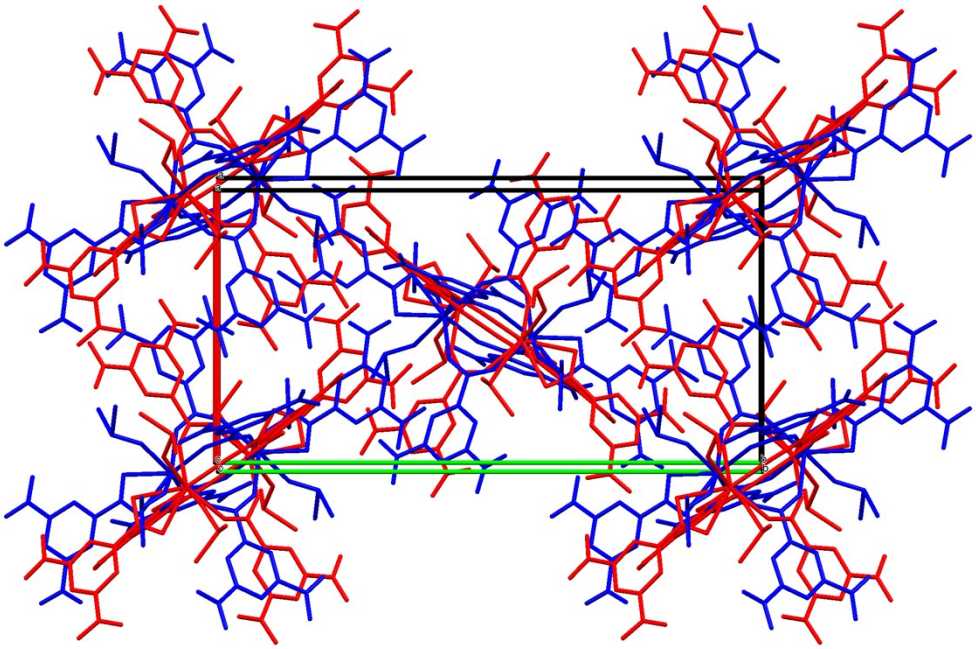

c

Fig. S2. Comparison of the structure of dimeric complexes in compounds **[$Tb_2(O_2CC_6H_3(NO_2)_2)_6(DMSO)_4$]·4DAD** (**3**) and **[$Tb_2(O_2CC_6H_3(NO_2)_2)_6(DMSO)_4$]·3($Me_2NPh$)** (a), and comparison of the crystal packings of the compounds; the projections along the axes b (b) and c (c).

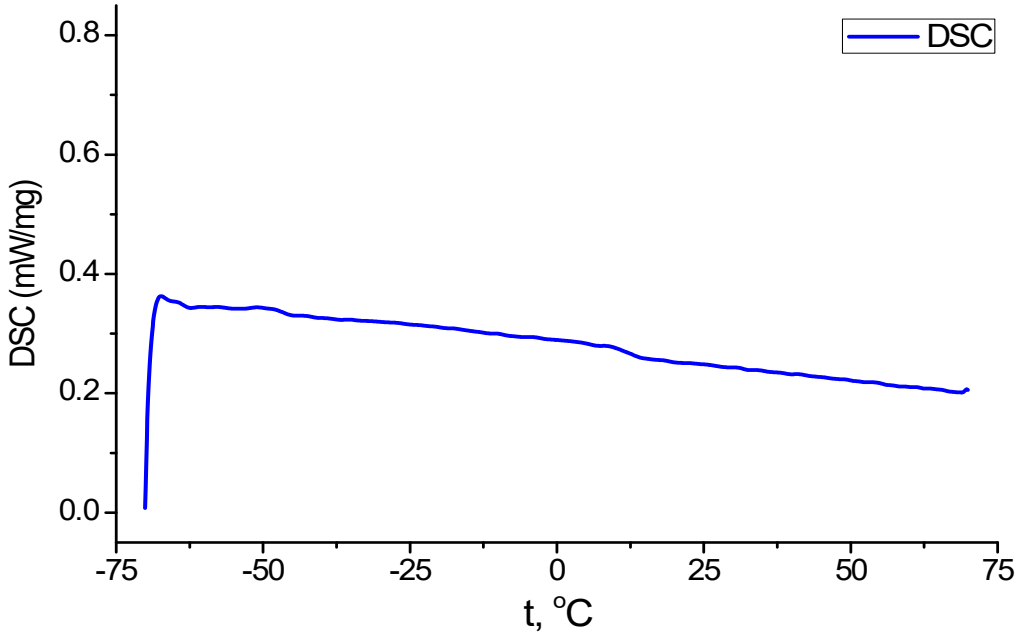

Fig. S3. DSC data for Gd complex **2** in -70 – 70 °C temperature range.

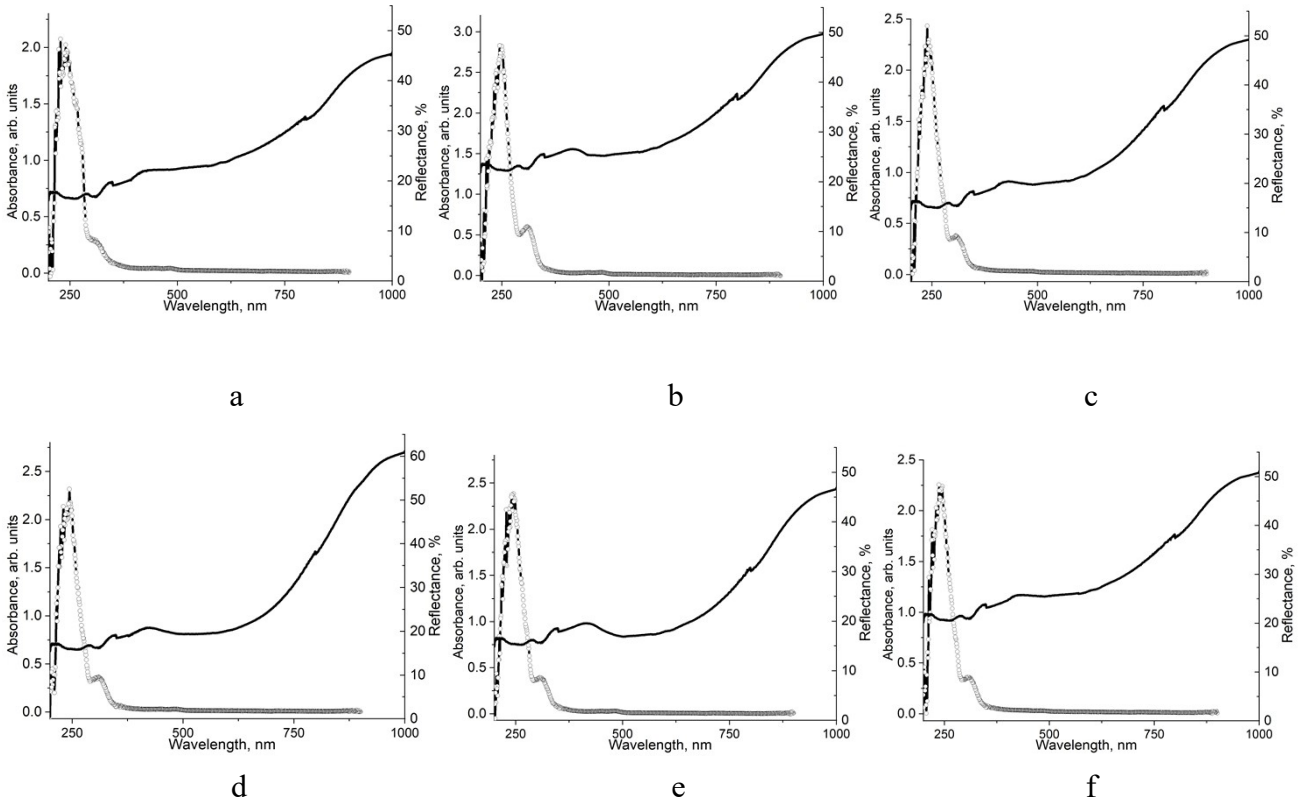

Fig. S4. Absorption UV–Vis spectra of 10^{-4} M THF solutions (-○-) and reflectance spectra of the powder samples (solid lines) of complexes **1**-**6**.

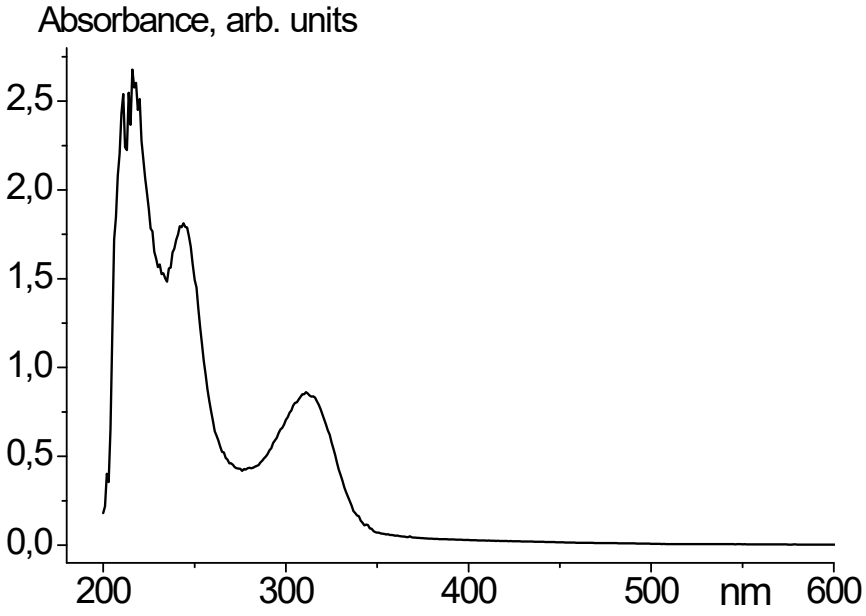

Fig. S5. Absorption UV–Vis spectrum of THF solution of DAD, 2×10^{-3} M

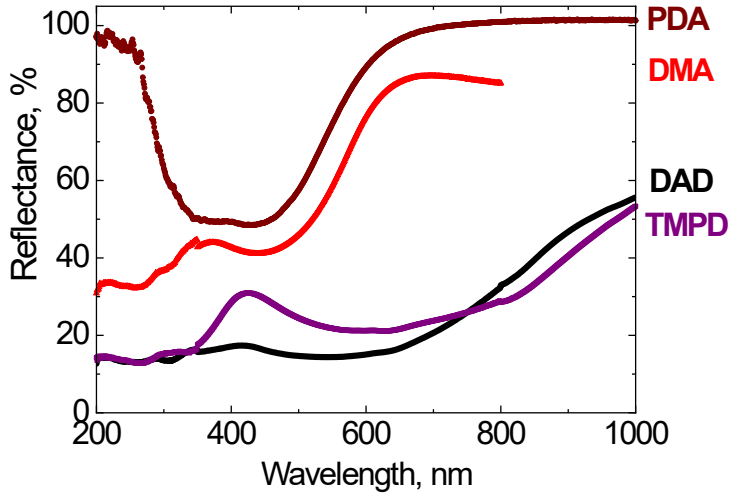

a

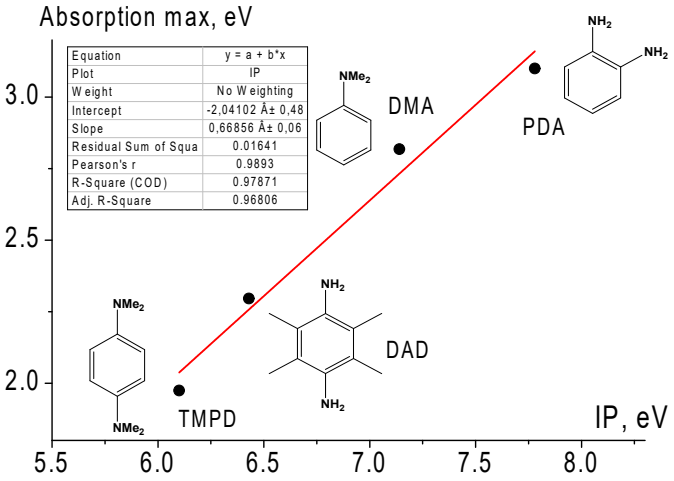

b

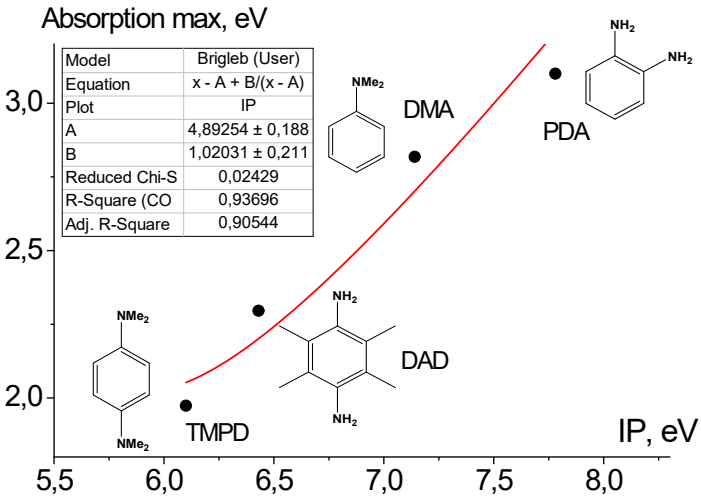

c

Fig. S6. Reflectance spectra of the solid-state samples of CT complexes of lanthanide 3,5-dinitrobenzoates with different donors (a) and correlation between the ionization potentials and the reflectance minima for the complexes with different electron donors obtained using the linear function (b) and using the hyperbolic formula given in the work [Briegleb, G. and Czekalla, J., *Z. Elektrochem.*, 1959, vol. 63, 1, p. 6-12] (c). The following relationship between wavelength and energy was used: $hv = 1239.8\ \lambda^{-1}$.

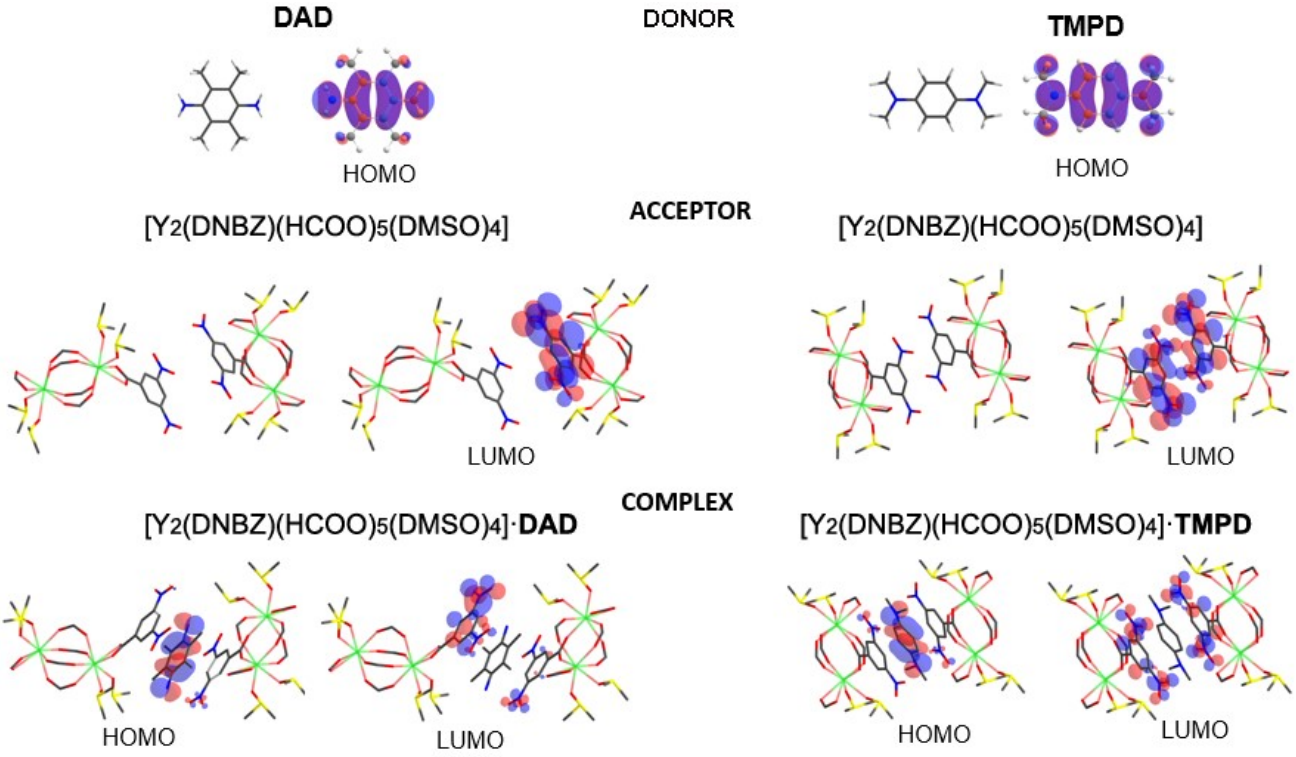

Fig. S7. Scheme of MO of donors (DAD, TMPD), DNBZ acceptors, and complexes.

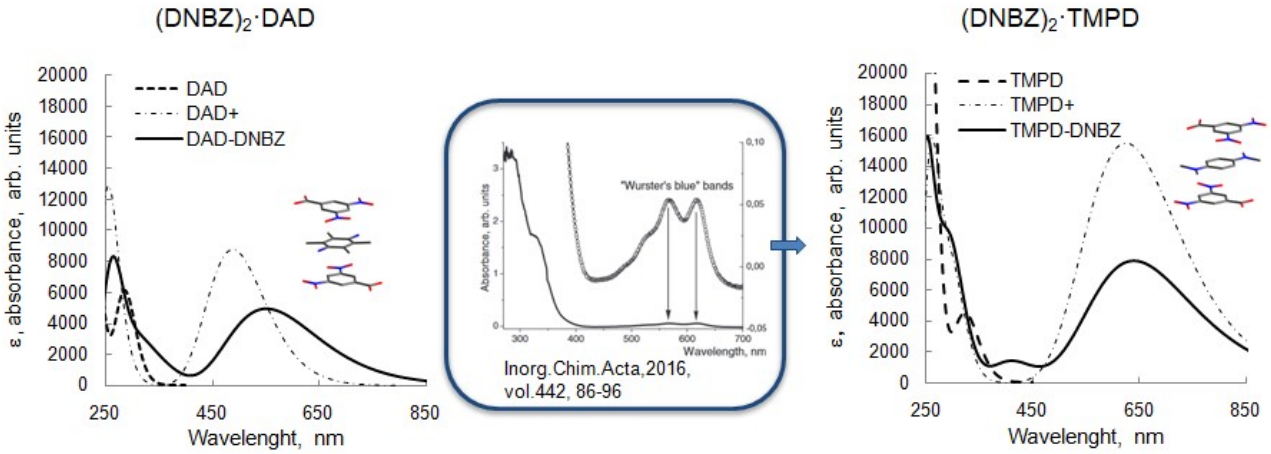

Fig. S8. Calculated UV-Vis spectra taking into account the solvent (THF) in the conductor-like polarizable continuum model (CPCM) model.

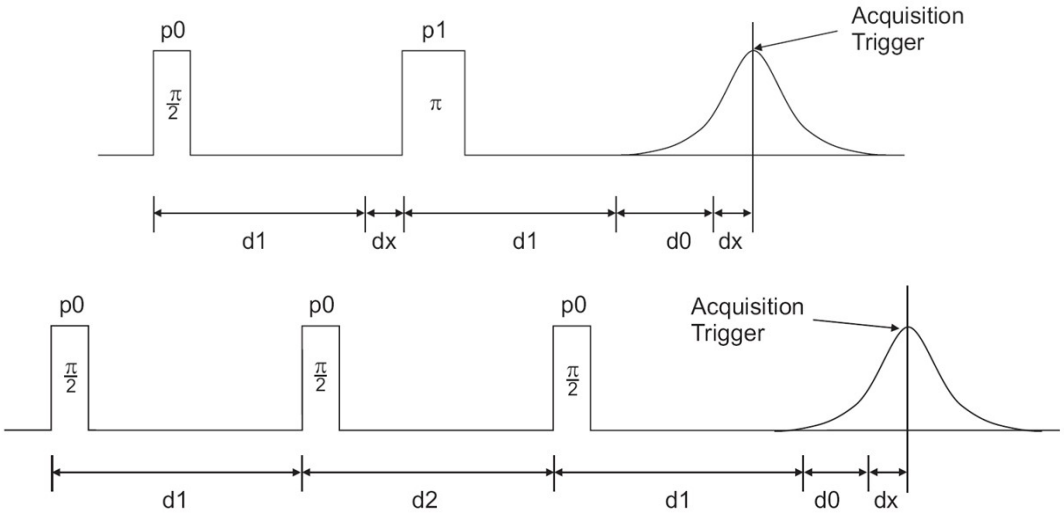

Fig. S9. 2-pulse (top) and 3-pulse (bottom) schemes for spin echo generating.

ESEEM study details.

Several types of ESEEM experiments with different pulse sequences were employed, with appropriate phase cycling schemes to eliminate unwanted features from experimental echo envelopes. Among them are two pulse and 1D and 2D three- and four-pulse sequences. In the two-pulse electron spin echo (ESE) experiment (π/2-τ-π-τ-echo), intensity of the echo signal at a fixed interval, τ, between two microwave pulses with spin vector rotation angles π/2 and π is measured as a function of magnetic field. In the 1D three-pulse experiment (π/2-τ-π/2- T-π/2-τ-echo), the intensity of the stimulated echo signal after the third pulse is recorded as a function of time, T, at constant time, τ. The set of three-pulse envelopes recorded at different τ values form a 2D three-pulse data set. In the 1D four-pulse experiment (π/2-τ-π/2-t_1-π-t_2-π/2-τ-echo), the intensity of the stimulated echo after the fourth pulse was measured with variation of t_2 and t_1 whilst τ remained constant. The length of a π/2 pulse was nominally 16 ns and a π pulse – 32 ns. The repetition rate of pulse sequences was 1000 Hz. For the 2D HYSCORE X-band spectra, the pulsed echo amplitude was measured using the sequence $\pi/2$-τ-$\pi/2$-t_1-π-t_2-$\pi/2$-τ-echo with an τ value of 136/200 ns and an 40/44 ns detector gate width (centered at the maximum of the echo signal); the delays were defined as the differences in the starting points of the pulses.[1] The echo intensity was measured as a function of t_1 and t_2, where t_1 and t_2 were incremented in steps of 20 ns or 32 ns from their initial values of 88 ns or 100 ns, respectively. Equal amplitude pulses of 16 ns for $\pi/2$ and 32 ns for π were used to record a 256×256 matrix. The 16 ns time difference between the initial values of t_1 and t_2 and $\pi/2$ and π were set equal to obtain more symmetric spectra. In Q-band experiments, equal amplitude pulses of 8 ns for $\pi/2$ and 16 ns for π were used. The unwanted echoes and anti-echoes were eliminated by applying a 4-step or 8-step phase cycling procedure.[2]

For the 2D HYSCORE data, a low-order polynomial baseline correction and tapering with a Hamming (Hanning and cosine) function was used to remove the unwanted echo decay. Before the application of a 2D Fourier (forward) transform, the data was zero filled to a 1024×1024 matrix, and the 2D HYSCORE spectral contour plots were created using Matlab R2021a.

[1] A. Schweiger and Jeschke, G. Principles of Pulse Electron Paramagnetic Resonance, Oxford University Press, Oxford, 2001.

[2] C. Gemperle, G. Aebli, A. Schweiger, and R. R. Ernst, Phase cycling in pulse EPR, *J. Magn. Reson.*, 1990, **88**, 241-256.

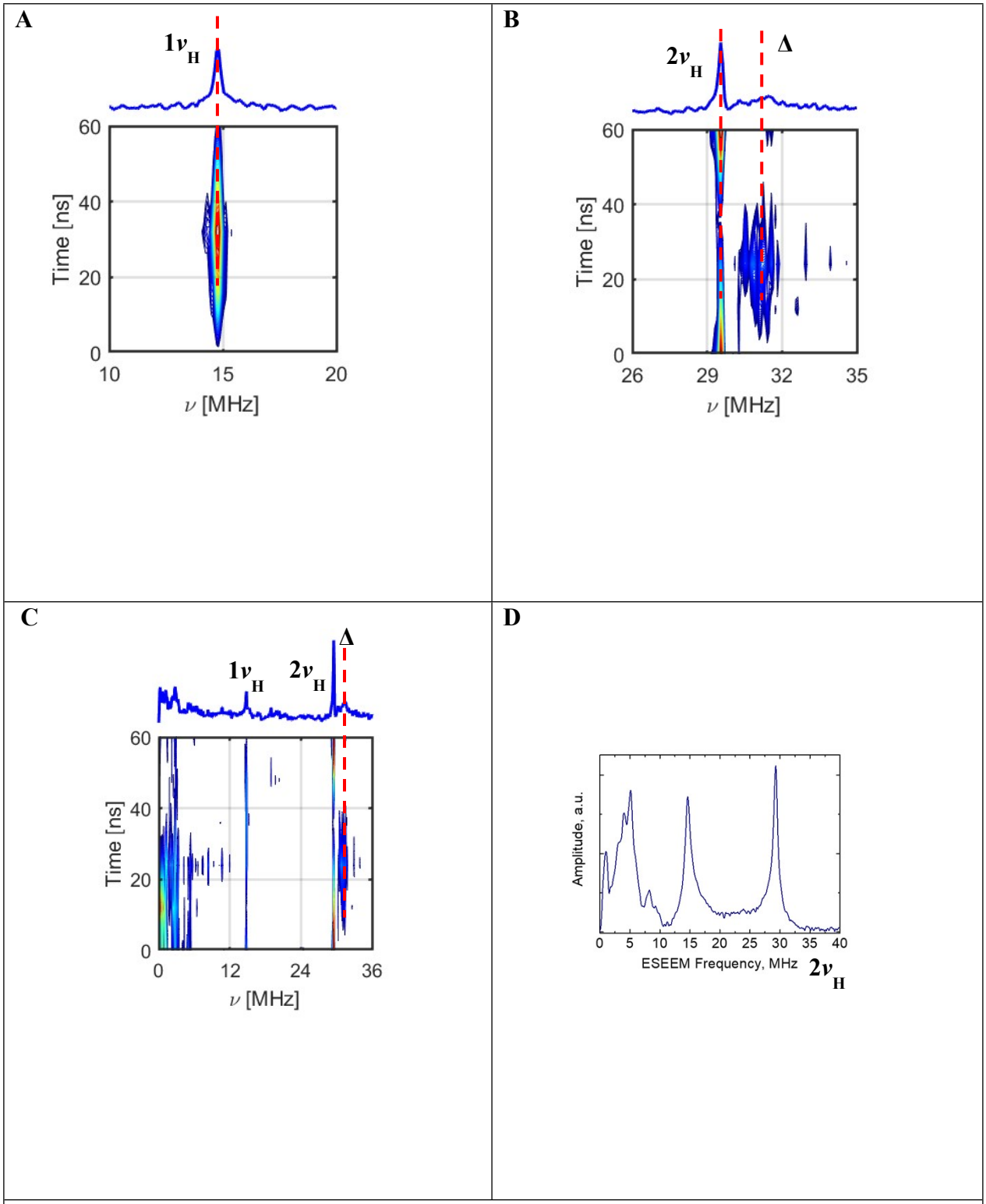

Fig. S10. Contour peaks of four-pulse 2D ESEEM sum combinations spectra of complex **7** (347.9 mT, step 12 ns, τ = 100 ns, 9.7284 GHz, 12 K). **A)** The narrow range shows $1\nu_H$ peak (the single-quantum transition) in the interval of 14.5 - 15.5 MHz. **B)** There is a significant anisotropic hyperfine coupling for the protons contributing to the contour lines shifted from $2\nu_H$ peak (the double-quantum) at ~29.5 MHz. The relative intensity of the $2\nu_H$ peak and shifted peaks do not change at different pulse delay t time, indicating a similar distribution of the protons in the complex **7** environment. **C)** The broad range is displayed in the frequency interval of 0 – 36 MHz. **D)** Two-pulse 1D ESEEM is comparable to spectra side-by-side (Fig. 7 in the main text, just comparing).

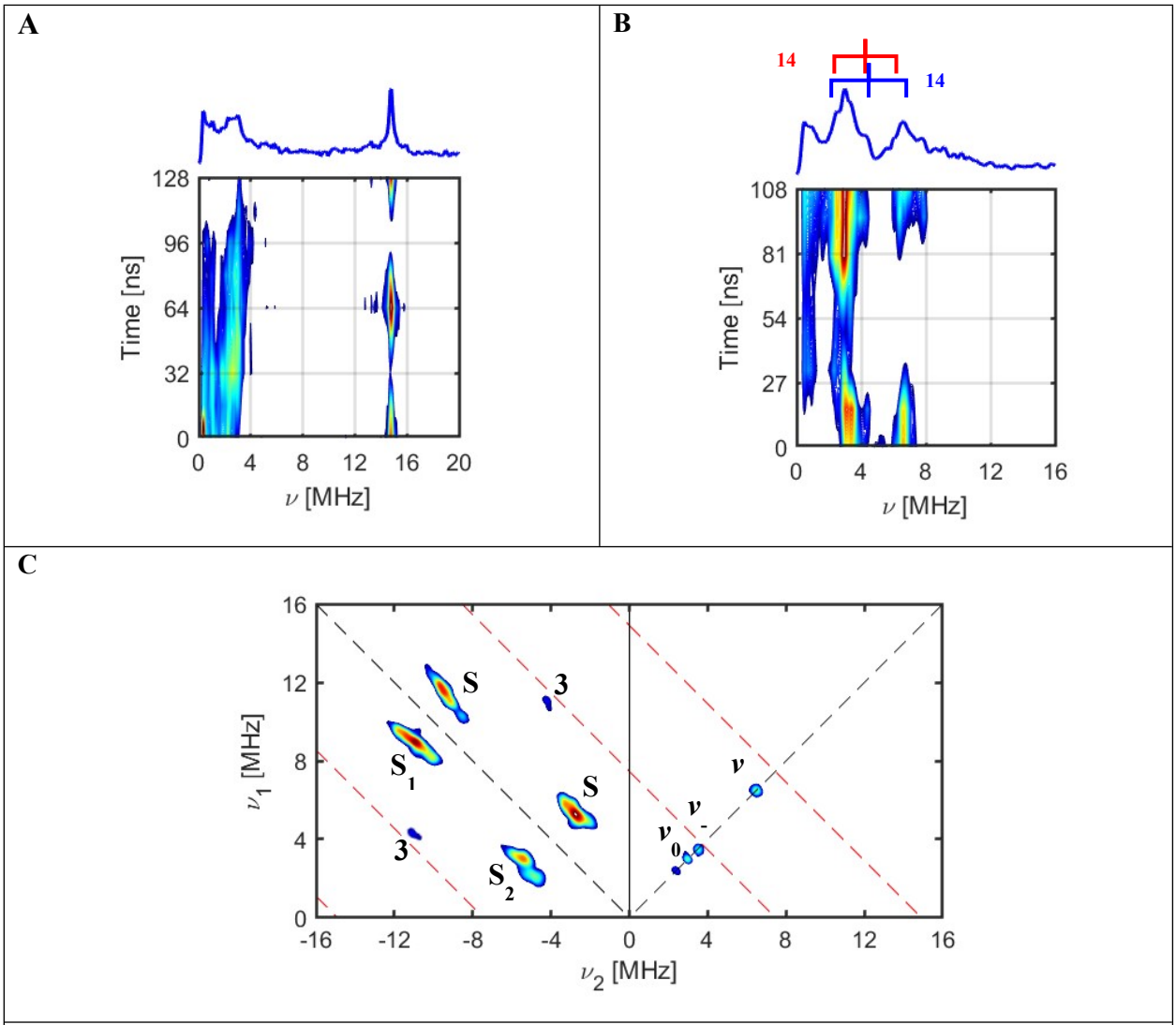

Fig. S11. Contour representations of 2D ESEEM spectra of complex **7**. **A)** Three-pulse 2D ESEEM spectrum collected at 16 K (X-band, 9.7284 GHz, 347.9 mT, τ = 100 ns). Nuclear quadrupole transition peaks strongly overlap in the region of 0.3 - 4.3 MHz, while Larmor frequency peak of protons is at ~15 MHz. **B)** Three-pulse 2D ESEEM spectrum at 298 K (Q-band, 33.9697 GHz, 1211.4 mT, τ = 100 ns). Nuclear quadrupole transition peaks are now overlapped in the region of 1.0 - 8.5 MHz. **C)** 2D HYSCORE spectrum at 298 K (Q-band, 33.9697 GHz, 1211.4 mT, τ = 136 ns, step 32 ns). In (+,+) quadrant, three transition frequencies of ^{14}N quadrupole interactions are also overlapped. In (-,+) quadrant, the correlation peaks of single-quantum transitions of two-coupled ^{14}N nuclei are partially resolved. Red dashed lines represent the single- and double-quantum transitions of coupled ^{14}N nuclei.

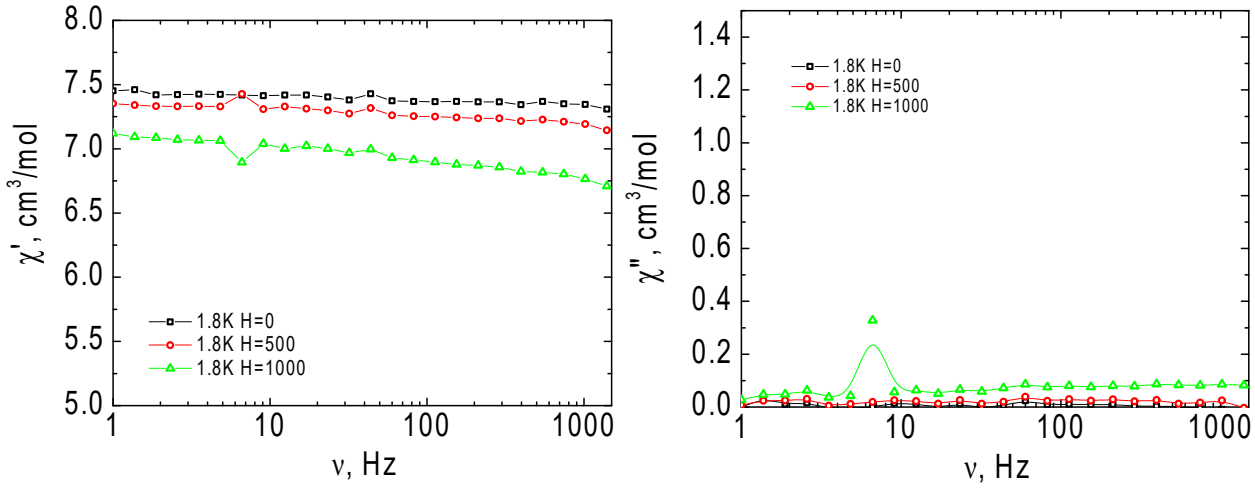

Fig. S12. Frequency dependencies of the in-phase (left) and out-of-phase (right) ac-magnetic susceptibility for complex **3** (Tb) at 1.8 K taken under 0 (black), 500 (red), and 1000 Oe (green) dc-field. Solid lines are visual guides.

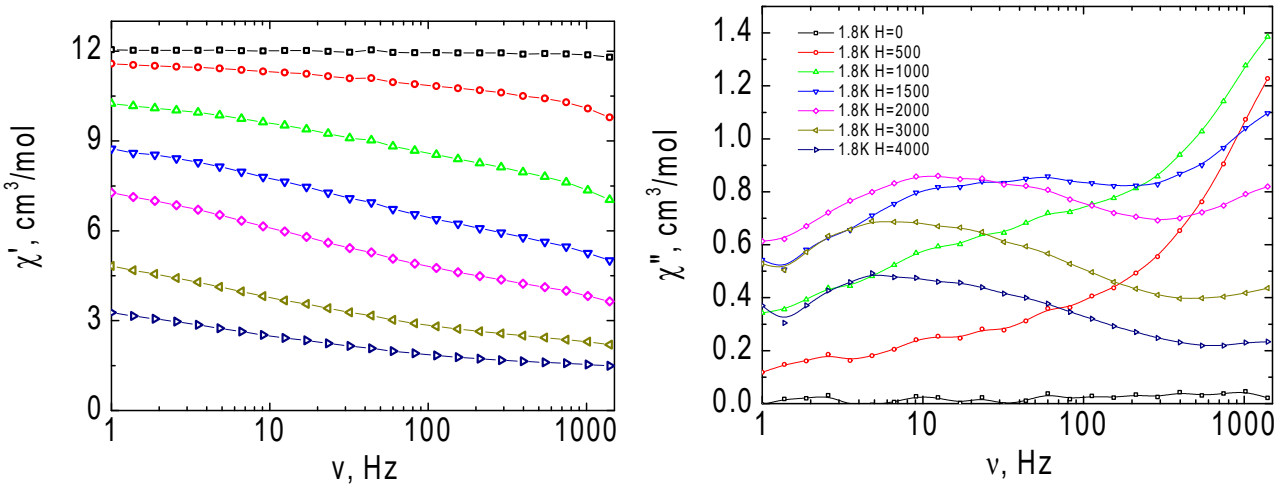

Fig. S13. Frequency dependencies of the in-phase (left) and out-of-phase (right) ac-magnetic susceptibility for complex **4** (Dy) at 1.8 K taken under different dc-fields. Solid lines are visual guides.

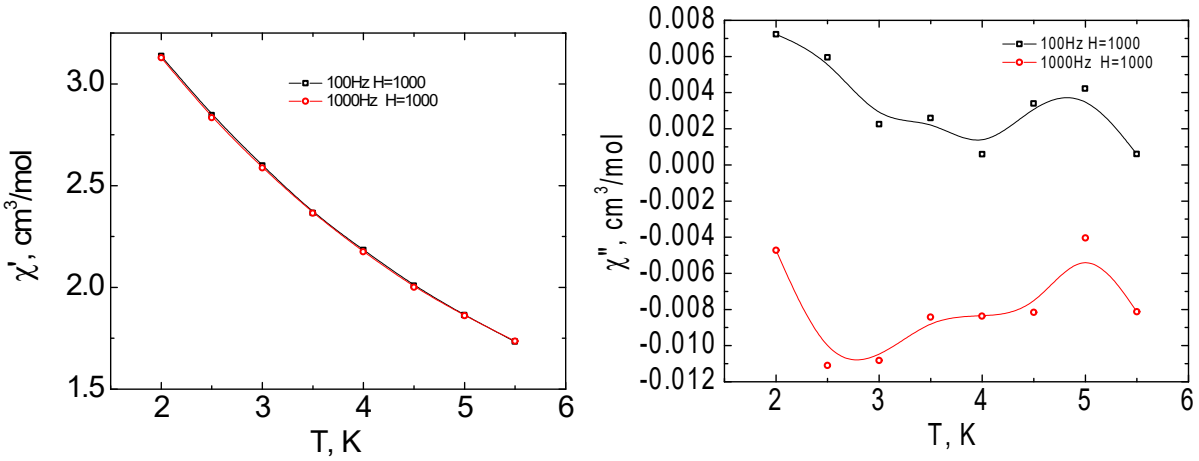

Fig. S14. Temperature dependencies of the in-phase (left) and out-of-phase (right) ac-magnetic susceptibility for complex **5** (Ho) in the 2-5.5 K range under 1000 Oe *dc*-field. Solid lines are visual guides.

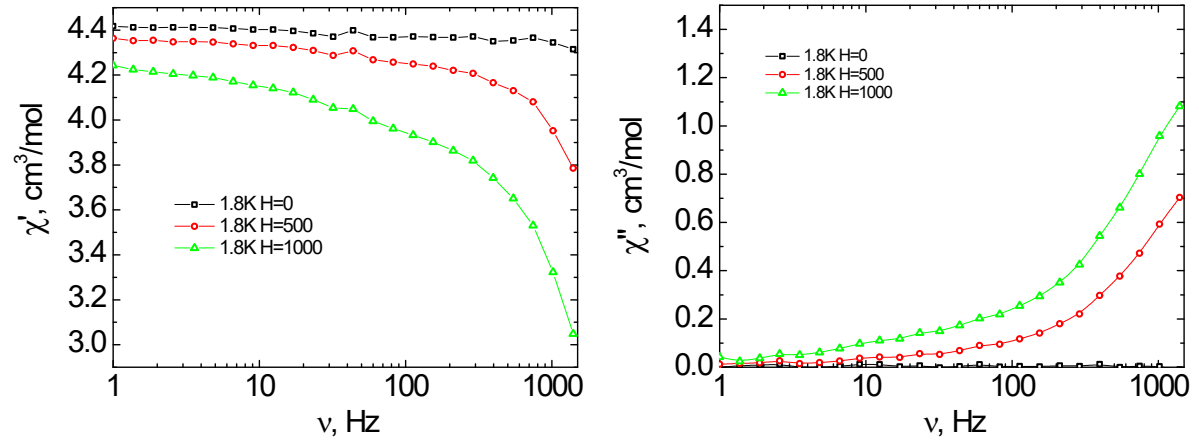

Fig. S15. Frequency dependencies of the in-phase (left) and out-of-phase (right) ac-magnetic susceptibility for complex **6** (Er) at 1.8 K taken under different dc-fields. Solid lines are visual guides.

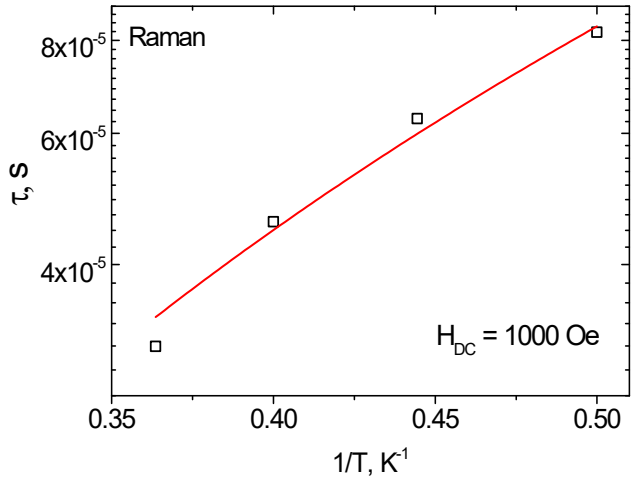

a

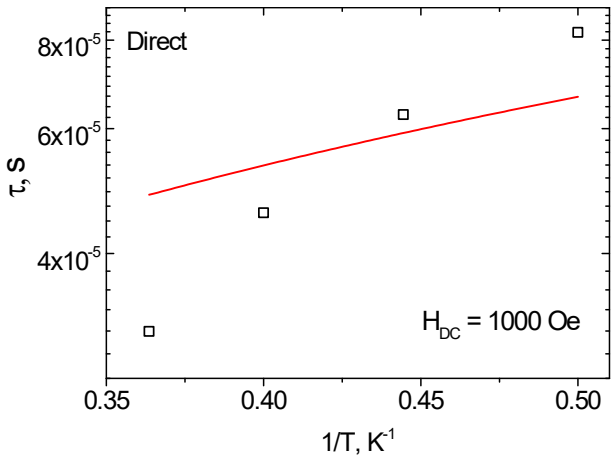

b

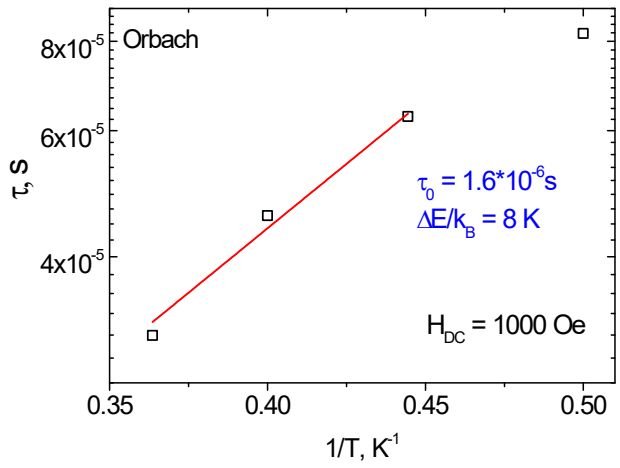

c

Fig. S16. The τ *vs.* T^{-1} plot for **4** in 1000 Oe *dc*-field. The red lines represent the best fits using Orbach (a), Raman (b), and direct (c) mechanisms.

Table S4. Fitting of the *τ vs. 1/T* dependences for complex **4**.

Dependence of the relaxation time τ on the reciprocal temperature for complex **4** (H = 1.0 kOe, T = 2.00-2.75 K).	Fit function, temperature range, and the best-fit parameters with uncertainties.
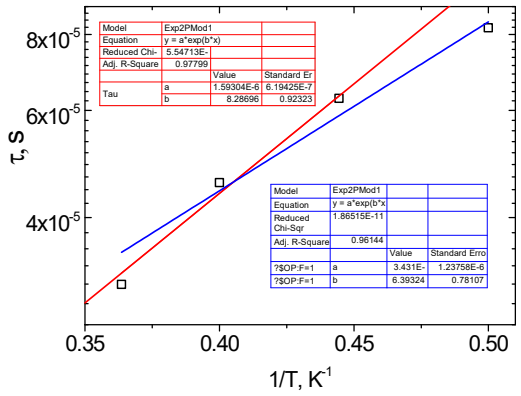	**Orbach** $\tau = \tau_0 \cdot \exp(\Delta E/kT)$ T = 2.25-2.75 K $\Delta E/k$ = 8.3 ± 0.9 K $\tau_0 = 1.6 \cdot 10^{-6} \pm 6.2 \cdot 10^{-7}$ s R^2 = 0.9780 (red line) T = 2.00-2.75 K $\Delta E/k$ =6.4 ± 0.8 K $\tau_0 = 3.4 \cdot 10^{-6} \pm 1.2 \cdot 10^{-6}$ s R^2 = 0.9614 (blue line) The values of relaxation times characteristic of over-barrier one-phonon remagnetization corresponding to the Orbach mechanism should be in the range of ~ 10^{-10} – 10^{-12} s. [1]
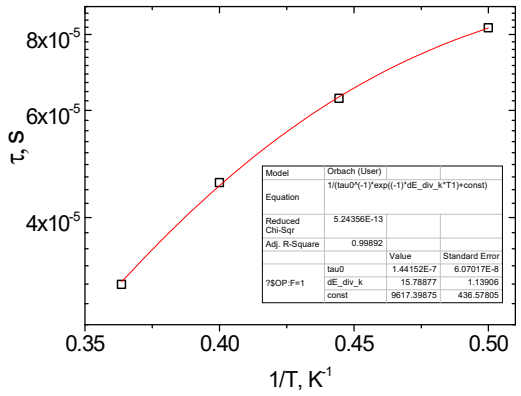	**Orbach+ QTM** $\tau^{-1} = \tau_0^{-1} \cdot \exp(-\Delta E/kT) + B$ $\Delta E/k$ = 15.8 ± 1.1 K $\tau_0 = 1.4 \cdot 10^{-7} \pm 6.1 \cdot 10^{-8}$ s B= 9617 ± 436 s^{-1} R^2 = 0.9989 The values of relaxation times characteristic of over-barrier one-phonon remagnetization corresponding to the Orbach mechanism should be in the range of ~ 10^{-10} – 10^{-12} s. One of the most adequate parameter values from physical point of view. [1]
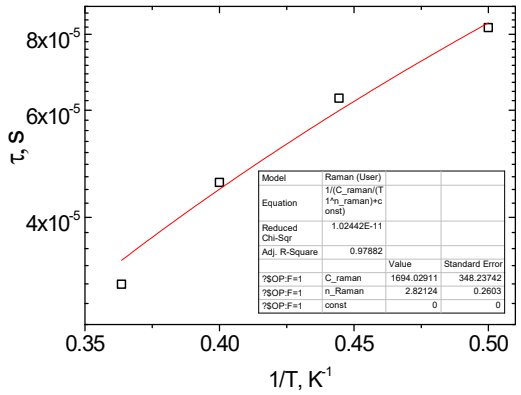	**Raman** $\tau^{-1} = C_{Raman} T^{n\_Raman}$ C_{Raman}= 1694 ± 348 $s^{-1}K^{-nRaman}$ n_{Raman}= 2.8 ± 0.3 R^2 = 0.9996 The values of the C_{Raman} parameter should be in the range of 10^{-5} - 10^{-1} $K^{-n\_Raman}s^{-1}$. [1]

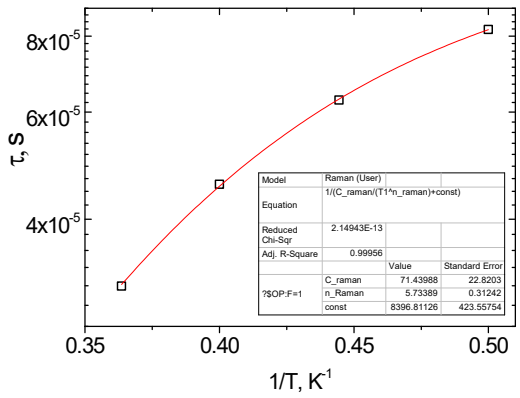

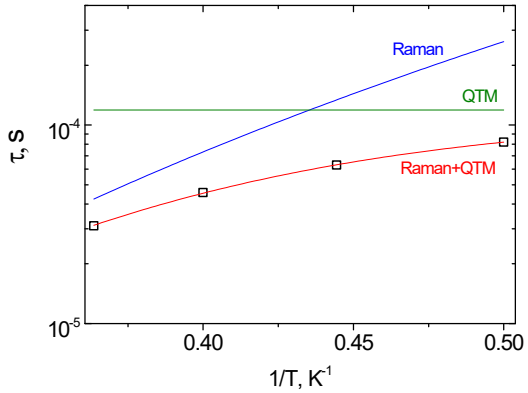

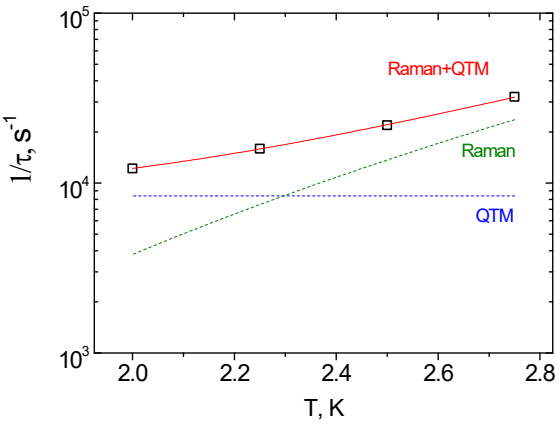

Raman+ QTM

$\tau^{-1} = C_{Raman} T^{nRaman} + B$

C_{Raman}= 71.4 ± 22.8 s^{-1} $K^{-nRaman}$
n_{Raman}= 5.7 ± 0.3
B = 8397 ± 424 s^{-1}
R^2 = 0.9996

The values of the C_{Raman} parameter should be in the range of 10^{-5} - 10^{-1} $K^{-n\_Raman}s^{-1}$. [1]

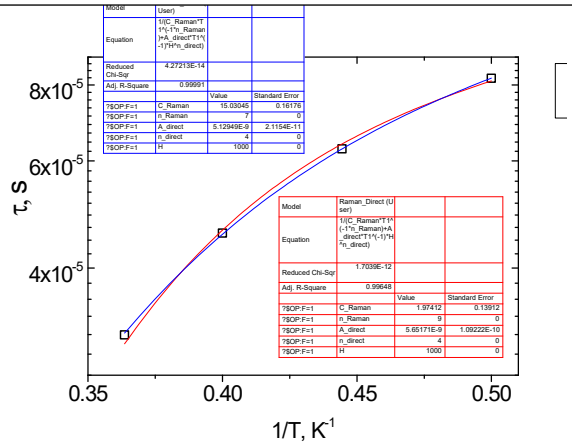

Raman+Direct

$\tau^{-1} = C_{\text{Raman}} T^{\text{nRaman}} + A_{direct} T H^4$

C_{Raman}= 1.97 ± 0.14 $s^{-1}K^{-\text{nRaman}}$
n_{Raman}=9 (red line)
A_{direct} = 5.7·10^{-9} ± 1.1·10^{-10} $K^{-1}Oe^{-4}s^{-1}$
R^2 = 0.9965

The values of the C_{Raman} parameter should be in the range of 10^{-5} - 10^{-1} $K^{-n\_Raman}s^{-1}$. One of the most adequate parameter values from physical point of view. [1]

C_{Raman}= 15.0 ± 0.2 $s^{-1}K^{-\text{nRaman}}$
n_{Raman}=7 (blue line)
A_{direct} = 5.1·10^{-9} ± 2.1·10^{-11} $K^{-1}Oe^{-4}s^{-1}$
R^2 = 0.9999

The values of the C_{Raman} parameter should be in the range of 10^{-5} - 10^{-1} $K^{-n\_Raman}s^{-1}$. [1]

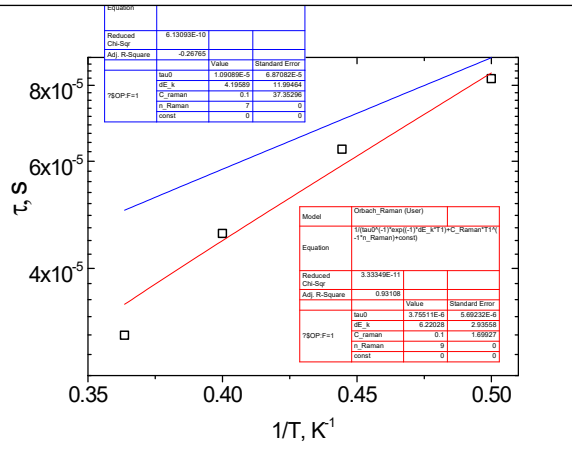

Orbach+Raman

$\tau^{-1} = \tau_0^{-1} \cdot \exp(-\Delta E/kT) + C_{\text{Raman}} T^{\text{nRaman}}$

$\Delta E/k$ = 6.2 ± 2.9 K
τ_0 = 3.8·10^{-6} ± 5.7·10^{-6} s
C_{Raman}= 0.1 ± 1.7 $s^{-1}K^{-\text{nRaman}}$
n_{Raman}= 9 (red line)
R^2 = 0.9311
The errors exceed he calculated values.

$\Delta E/k$ = 4.2 ± 12.0 K
τ_0 = 1.1·10^{-5} ± 6.9·10^{-5} s
C_{Raman}= 0.1 ± 37.3 $s^{-1}K^{-\text{nRaman}}$
n_{Raman}= 7 (blue line)
R^2 = -0.2677 (?)
The errors exceed he calculated values.

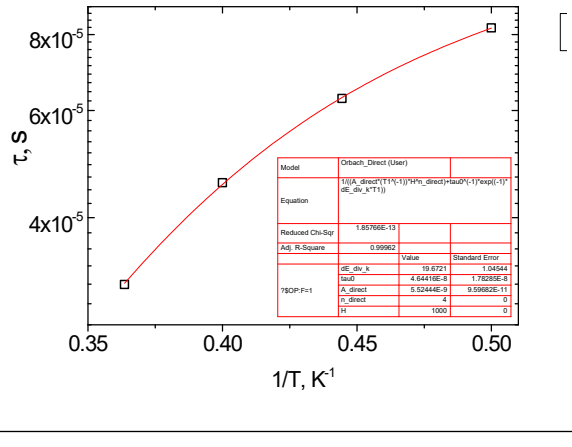

Orbach+Direct

$\tau^{-1} = \tau_0^{-1} \cdot \exp(-\Delta E/kT) + A_{direct} T H^4$

$\Delta E/k$ = 19.7 ± 1.0 K
τ_0 = 4.6·10^{-8} ± 1.8·10^{-8}s
A_{direct} = 5.5·10^{-9} ± 9.6·10^{-11} $K^{-1}Oe^{-4}s^{-1}$
R^2 = 0.9996

The values of relaxation times characteristic of over-barrier one-phonon remagnetization corresponding to the Orbach mechanism should be in the range of ~ 10^{-10} – 10^{-12} s. One of the most adequate parameter values from physical point of view. [1]

[1] N.N. Efimov, K.A. Babeshkin, A.V. Rotov, Dynamic Magnetic Susceptibility Method in Studies of Coordination Compounds, *Russ. J. Coord. Chem.*, 2024, **50**, 363–373.

Elemental analysis data and IR spectra frequences for complexes 1-7.

For **1**, anal. calc. for $Sm_2C_{90}H_{106}N_{20}O_{40}S_4$: C, 42.61, H, 4.21, N 11.04. Found: C, 42.65, H, 4.17, N 11.07. IR of **1**: 3435 w, 3370w, 3098 w, 3001 w, 2916 w, 2866 w, 1671 m, 1621 m, 1609 m, 1572 w, 1529 s, 1457 m, 1396 s, 1338 vs, 1294 m, 1192 w, 1140 m, 1083 m, 1071 m, 1013 s, 956 m, 923 m, 913 m, 838 w, 790 m, 760 m, 721 vs, 708 vs, 632 m, 623 m, 593 m, 549 m, 520 m, 463 m.

For **2**, anal. calc. for $Gd_2C_{90}H_{106}N_{20}O_{40}S_4$: C, 42.38, H, 4.19, N 10.98. Found: C, 42.40, H, 4.20, N 10.95. IR of **2**: 3438 w, 3370w, 3097 w, 2995 w, 2913 w, 2862 w, 1673 s, 1623 m, 1607 m, 1572 w, 1531 s, 1456 m, 1398 vs, 1338 vs, 1272 m, 1192 w, 1146 w, 1085 m, 1072 m, 1015 s, 959 m, 922 m, 915 m, 838 w, 790 m, 759 m, 731 s, 721 vs, 708 vs, 623 m, 593 m, 549 m, 520 m, 477 m, 460 m, 446 w.

For **3**, anal. calc. for $Tb_2C_{90}H_{106}N_{20}O_{40}S_4$: C, 42.32, H, 4.18, N 10.97. Found: C, 42.29, H, 4.14, N 10.95. IR of **2**: 3435 w, 3370w, 3097 w, 2992 w, 2914 w, 2859 w, 1675 s, 1623 m, 1607 m, 1572 w, 1529 s, 1456 m, 1398 vs, 1337 vs, 1272 m, 1191 w, 1150 w, 1085 m, 1072 m, 1015 s, 959 m, 922 m, 915 m, 838 w, 790 m, 759 m, 731 s, 721 vs, 708 vs, 623 m, 593 m, 544 m, 520 m, 472 w, 456 w, 449 w.

For **4**, anal. calc. for $Dy_2C_{90}H_{106}N_{20}O_{40}S_4$: C, 42.21, H, 4.17, N 10.94. Found: C, 42.25, H, 4.15, N 10.90. IR of **2**: 3437 w, 3370w, 3097 w, 2994 w, 2913 w, 2865 w, 1677 s, 1623 m, 1609 m, 1573 w, 1530 s, 1456 m, 1399 s, 1337 vs, 1272 m, 1191 w, 1147 w, 1083 m, 1072 m, 1015 s, 959 m, 922 m, 915 m, 838 w, 790 m, 759 m, 731 s, 721 vs, 708 vs, 623 m, 593 m, 551 m, 520 m, 479 w, 448 w.

For **5**, anal. calc. for $Ho_2C_{90}H_{106}N_{20}O_{40}S_4$: C, 42.13, H, 4.16, N 10.92. Found: C, 42.18, H, 4.11, N 10.88. IR of **2**: 3437 w, 3370w, 3097 w, 2991 w, 2914 w, 2862 w, 1678 s, 1623 m, 1609 m, 1573 w, 1529 s, 1457 s, 1399 s, 1337 vs, 1272 m, 1191 w, 1147 w, 1085 m, 1072 m, 1015 s, 960 m, 922 m, 915 m, 838 w, 790 m, 759 m, 731 s, 719 vs, 708 vs, 625 m, 593 m, 549 m, 523 m, 463 w, 450 w.

For **6**, anal. calc. for $Er_2C_{90}H_{106}N_{20}O_{40}S_4$: C, 42.05, H, 4.16, N 10.90. Found: C, 42.09, H, 4.14, N 10.95. IR of **2**: 3437 w, 3370w, 3097 w, 2991 w, 2914 w, 2860 w, 1679 s, 1623 m, 1609 m, 1573 w, 1529 s, 1457 s, 1401 s, 1338 vs, 1272 m, 1192 w, 1143 w, 1085 m, 1072 m, 1015 s, 960 m, 920 m, 918 m, 838 w, 790 m, 759 m, 731 s, 721 vs, 710 vs, 632 m, 625 m, 595 m, 543 m, 523 m, 462 w, 452 w.

For **7**, anal. calc. for $Y_2C_{90}H_{106}N_{20}O_{40}S_4$: C, 44.78, H, 4.43, N 11.60. Found: C, 44.82, H, 4.44, N 11.62. IR of **2**: 3435 w, 3370 w, 3097 w, 2992 w, 2913 w, 2862 w, 1680 s, 1623 m, 1609 m, 1573 w, 1529 s, 1457 s, 1401 s, 1337 vs, 1272 m, 1191 w, 1147 w, 1085 m, 1072 m, 1017 s, 960 m, 920 m, 915 m, 838 w, 790 m, 759 m, 731 s, 721 vs, 710 vs, 625 m, 595 m, 548 m, 520 m, 467 w, 456 w.

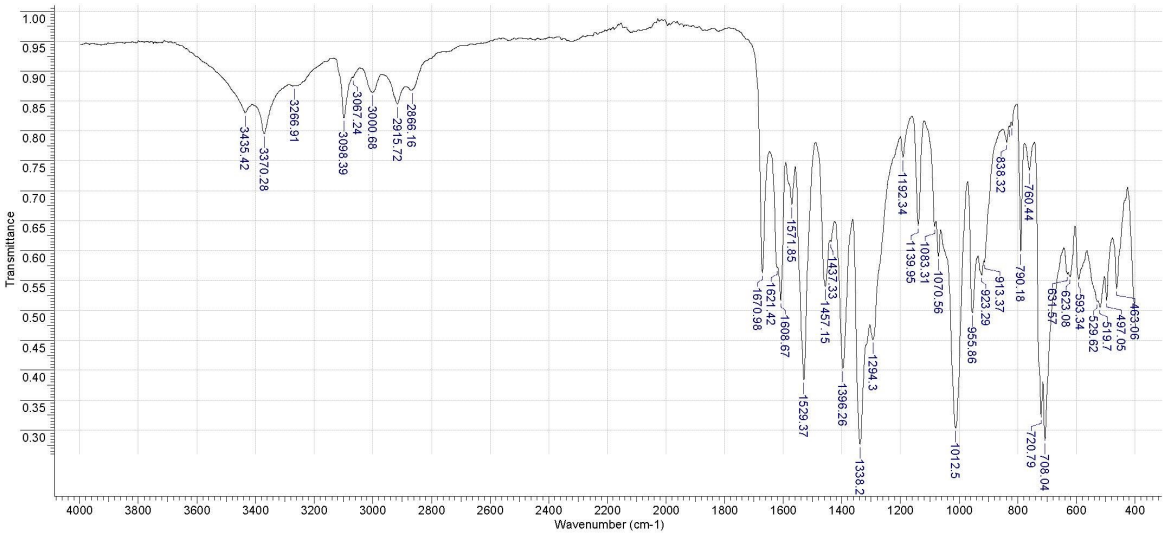

No	cm-1	T	Intensity	No	cm-1	T	Intensity	No	cm-1	T	Intensity
1	463.06	0.536	S	15	913.37	0.581	M	29	1571.85	0.677	M
2	497.05	0.517	S	16	923.29	0.559	S	30	1608.67	0.517	S
3	519.70	0.506	S	17	955.86	0.496	S	31	1621.42	0.571	M
4	529.62	0.515	S	18	1012.50	0.304	VS	32	1670.98	0.563	M
5	593.34	0.552	S	19	1070.56	0.590	M	33	2866.16	0.869	W
6	623.08	0.557	S	20	1083.31	0.640	M	34	2915.72	0.845	W
7	631.57	0.561	M	21	1139.95	0.641	M	35	3000.68	0.865	W
8	708.04	0.283	VS	22	1192.34	0.756	M	36	3067.24	0.889	W
9	720.79	0.322	VS	23	1294.30	0.451	S	37	3098.39	0.822	W
10	760.44	0.735	M	24	1338.20	0.276	VS	38	3266.91	0.876	W
11	790.18	0.599	M	25	1396.26	0.403	S	39	3370.28	0.796	W
12	819.91	0.809	W	26	1437.33	0.615	M	40	3435.42	0.831	W
13	826.99	0.806	W	27	1457.15	0.540	S				
14	838.32	0.781	W	28	1529.37	0.384	S				

a

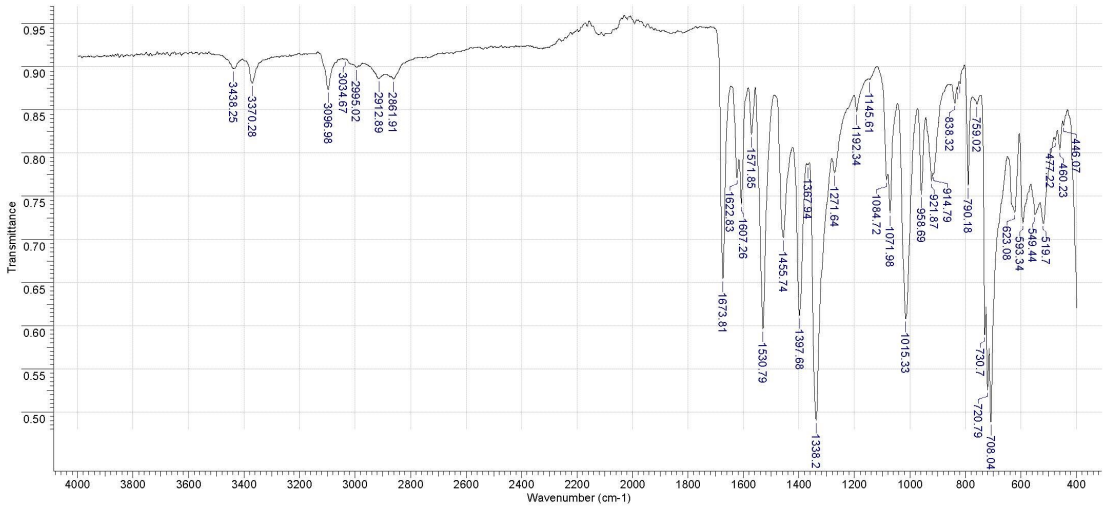

No	cm-1	T	Intensity	No	cm-1	T	Intensity	No	cm-1	T	Intensity
1	446.07	0.832	W	15	838.32	0.858	W	29	1530.79	0.596	S
2	460.23	0.804	M	16	914.79	0.775	M	30	1571.85	0.822	W
3	477.22	0.815	M	17	921.87	0.768	M	31	1607.26	0.741	M
4	519.70	0.719	M	18	958.69	0.752	M	32	1622.83	0.772	M
5	549.44	0.729	M	19	1015.33	0.608	S	33	1673.81	0.654	S
6	593.34	0.719	M	20	1071.98	0.731	M	34	2861.91	0.886	W
7	623.08	0.731	M	21	1084.72	0.769	M	35	2912.89	0.886	W
8	708.04	0.488	VS	22	1145.61	0.885	W	36	2995.02	0.899	W
9	720.79	0.525	VS	23	1192.34	0.848	W	37	3034.67	0.909	W
10	730.70	0.590	S	24	1271.64	0.777	M	38	3096.98	0.873	W
11	759.02	0.857	W	25	1338.20	0.490	VS	39	3370.28	0.881	W
12	790.18	0.763	M	26	1367.94	0.786	M	40	3438.25	0.898	W
13	819.91	0.880	W	27	1397.68	0.612	S				
14	828.41	0.873	W	28	1455.74	0.702	M				

b

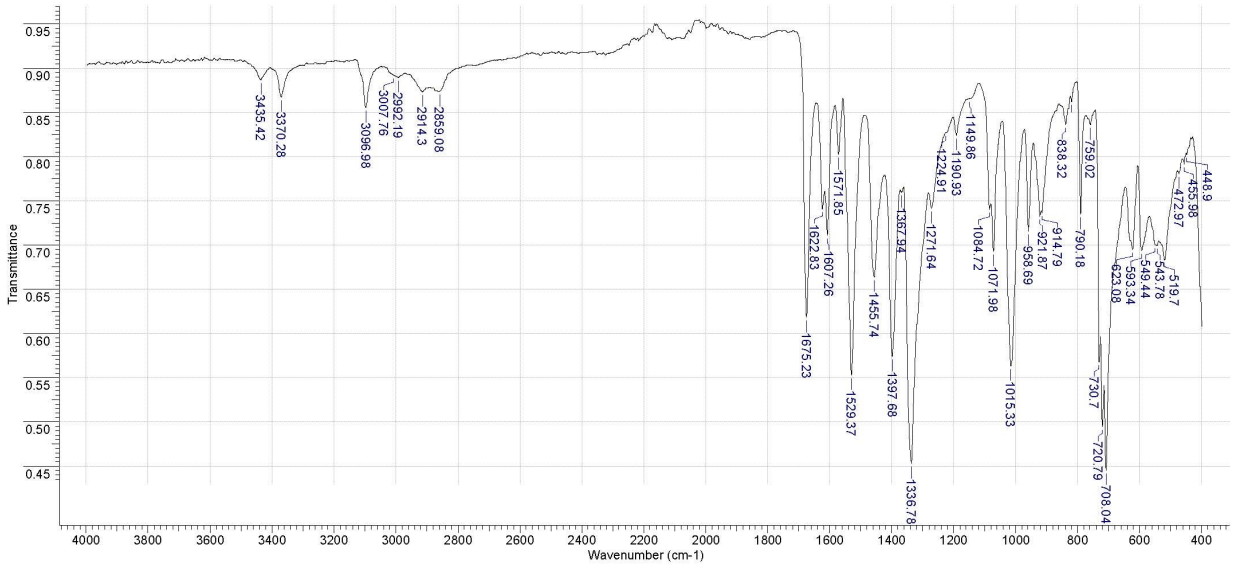

No	cm-1	T	Intensity
1	448.90	0.802	W
2	455.98	0.792	M
3	472.97	0.781	M
4	519.70	0.684	M
5	543.78	0.700	M
6	549.44	0.700	M
7	593.34	0.693	M
8	623.08	0.695	M
9	708.04	0.446	VS
10	720.79	0.495	VS
11	730.70	0.568	S
12	759.02	0.836	W
13	790.18	0.735	M
14	819.91	0.862	W

No	cm-1	T	Intensity
15	838.32	0.836	W
16	914.79	0.736	M
17	921.87	0.732	M
18	958.69	0.716	M
19	1015.33	0.563	S
20	1071.98	0.693	M
21	1084.72	0.740	M
22	1149.86	0.866	W
23	1190.93	0.824	W
24	1224.91	0.827	W
25	1271.64	0.741	M
26	1336.78	0.453	VS
27	1367.94	0.759	M
28	1397.68	0.574	S

No	cm-1	T	Intensity
29	1455.74	0.664	M
30	1529.37	0.553	S
31	1571.85	0.802	W
32	1607.26	0.711	M
33	1622.83	0.741	M
34	1675.23	0.618	S
35	2859.08	0.874	W
36	2914.30	0.873	W
37	2992.19	0.890	W
38	3007.76	0.892	W
39	3096.98	0.856	W
40	3370.28	0.867	W
41	3435.42	0.887	W

c

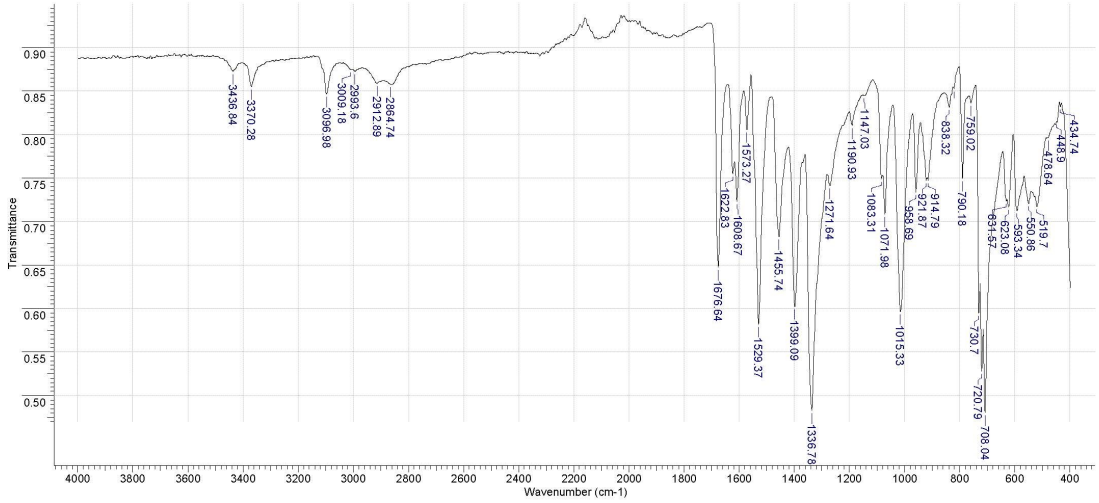

No	cm-1	T	Intensity
1	434.74	0.832	W
2	448.90	0.815	W
3	478.64	0.796	M
4	519.70	0.717	M
5	550.86	0.721	M
6	593.34	0.713	M
7	623.08	0.716	M
8	631.57	0.724	M
9	708.04	0.481	VS
10	720.79	0.528	S
11	730.70	0.595	S
12	759.02	0.836	W
13	790.18	0.749	M

No	cm-1	T	Intensity
14	821.33	0.852	W
15	838.32	0.831	W
16	914.79	0.747	M
17	921.87	0.747	M
18	958.69	0.734	M
19	1015.33	0.597	S
20	1071.98	0.708	M
21	1083.31	0.749	M
22	1147.03	0.845	W
23	1190.93	0.810	W
24	1271.64	0.741	M
25	1336.78	0.483	VS
26	1399.09	0.602	S

No	cm-1	T	Intensity
27	1455.74	0.682	M
28	1529.37	0.582	S
29	1573.27	0.806	W
30	1608.67	0.723	M
31	1622.83	0.755	M
32	1676.64	0.647	S
33	2864.74	0.858	W
34	2912.89	0.859	W
35	2993.60	0.872	W
36	3009.18	0.875	W
37	3096.98	0.847	W
38	3370.28	0.855	W
39	3436.84	0.873	W

d

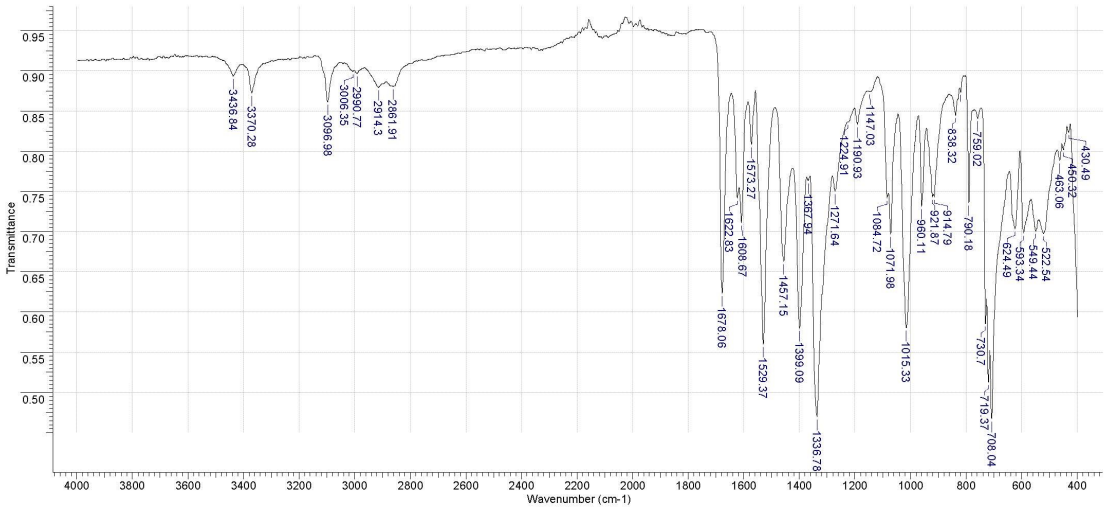

No	cm-1	T	Intensity
1	430.49	0.824	W
2	450.32	0.802	M
3	463.06	0.788	M
4	522.54	0.698	M
5	549.44	0.700	M
6	593.34	0.698	M
7	624.49	0.703	M
8	708.04	0.467	VS
9	719.37	0.513	VS
10	730.70	0.585	S
11	759.02	0.841	W
12	790.18	0.736	M
13	819.91	0.873	W
14	838.32	0.845	W

No	cm-1	T	Intensity
15	914.79	0.743	M
16	921.87	0.743	M
17	960.11	0.732	M
18	1015.33	0.580	S
19	1071.98	0.697	M
20	1084.72	0.742	M
21	1147.03	0.874	W
22	1190.93	0.833	W
23	1224.91	0.837	W
24	1271.64	0.750	M
25	1336.78	0.470	VS
26	1367.94	0.764	M
27	1399.09	0.580	S
28	1457.15	0.663	S

No	cm-1	T	Intensity
29	1529.37	0.560	S
30	1573.27	0.808	M
31	1608.67	0.711	M
32	1622.83	0.742	M
33	1678.06	0.623	S
34	2861.91	0.881	W
35	2914.30	0.879	W
36	2990.77	0.897	W
37	3006.35	0.900	W
38	3096.98	0.861	W
39	3370.28	0.873	W
40	3436.84	0.893	W

e

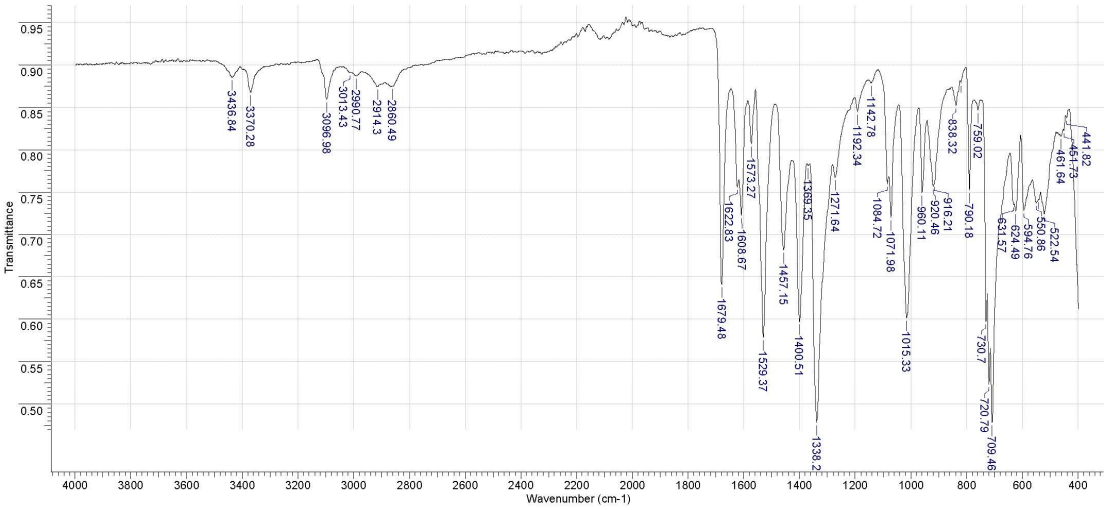

No	cm-1	T	Intensity
1	441.82	0.837	W
2	451.73	0.822	W
3	461.64	0.816	W
4	522.54	0.724	M
5	542.36	0.741	M
6	550.86	0.737	M
7	594.76	0.728	M
8	624.49	0.727	M
9	631.57	0.735	M
10	709.46	0.478	VS
11	720.79	0.523	VS
12	730.70	0.597	S
13	759.02	0.847	W
14	790.18	0.752	M

No	cm-1	T	Intensity
15	821.33	0.879	W
16	838.32	0.852	W
17	916.21	0.759	M
18	917.62	0.759	M
19	920.46	0.757	M
20	960.11	0.749	M
21	1015.33	0.602	S
22	1071.98	0.720	M
23	1084.72	0.760	M
24	1142.78	0.879	W
25	1192.34	0.845	W
26	1271.64	0.767	M
27	1338.20	0.479	VS
28	1369.35	0.781	M

No	cm-1	T	Intensity
29	1400.51	0.597	S
30	1457.15	0.681	M
31	1529.37	0.578	S
32	1573.27	0.807	M
33	1608.67	0.723	M
34	1622.83	0.756	M
35	1679.48	0.641	S
36	2860.49	0.875	W
37	2914.30	0.874	W
38	2990.77	0.887	W
39	3013.43	0.890	W
40	3096.98	0.859	W
41	3370.28	0.868	W
42	3436.84	0.885	W

f

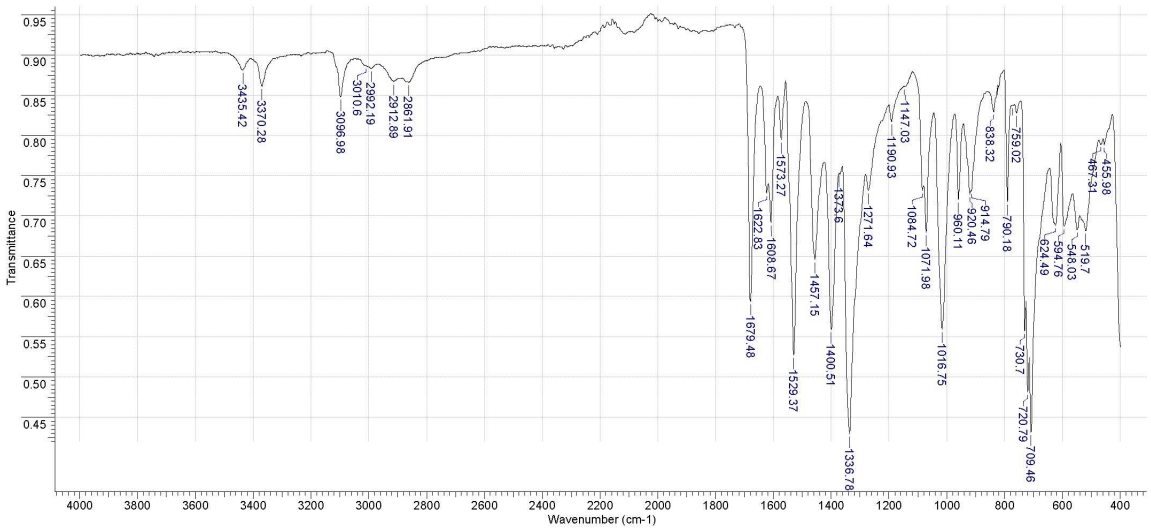

No	cm-1	T	Intensity	No	cm-1	T	Intensity	No	cm-1	T	Intensity
1	455.98	0.788	M	14	838.32	0.829	W	27	1457.15	0.646	M
2	467.31	0.789	M	15	914.79	0.730	M	28	1529.37	0.527	S
3	519.70	0.682	M	16	920.46	0.727	M	29	1573.27	0.795	M
4	548.03	0.683	M	17	960.11	0.720	M	30	1608.67	0.692	M
5	594.76	0.687	M	18	1016.75	0.559	S	31	1622.83	0.728	M
6	624.49	0.688	M	19	1071.98	0.680	M	32	1679.48	0.594	S
7	709.46	0.432	VS	20	1084.72	0.731	M	33	2861.91	0.866	W
8	720.79	0.481	VS	21	1147.03	0.861	W	34	2912.89	0.867	W
9	730.70	0.557	S	22	1190.93	0.817	W	35	2992.19	0.883	W
10	759.02	0.828	W	23	1271.64	0.732	M	36	3010.60	0.886	W
11	771.77	0.837	W	24	1336.78	0.429	VS	37	3096.98	0.848	W
12	790.18	0.718	M	25	1373.60	0.753	M	38	3370.28	0.861	W
13	824.16	0.863	W	26	1400.51	0.559	S	39	3435.42	0.881	W

g

Fig. S17. IR spectra of complexes **1**-**7** (a – g, resp.).

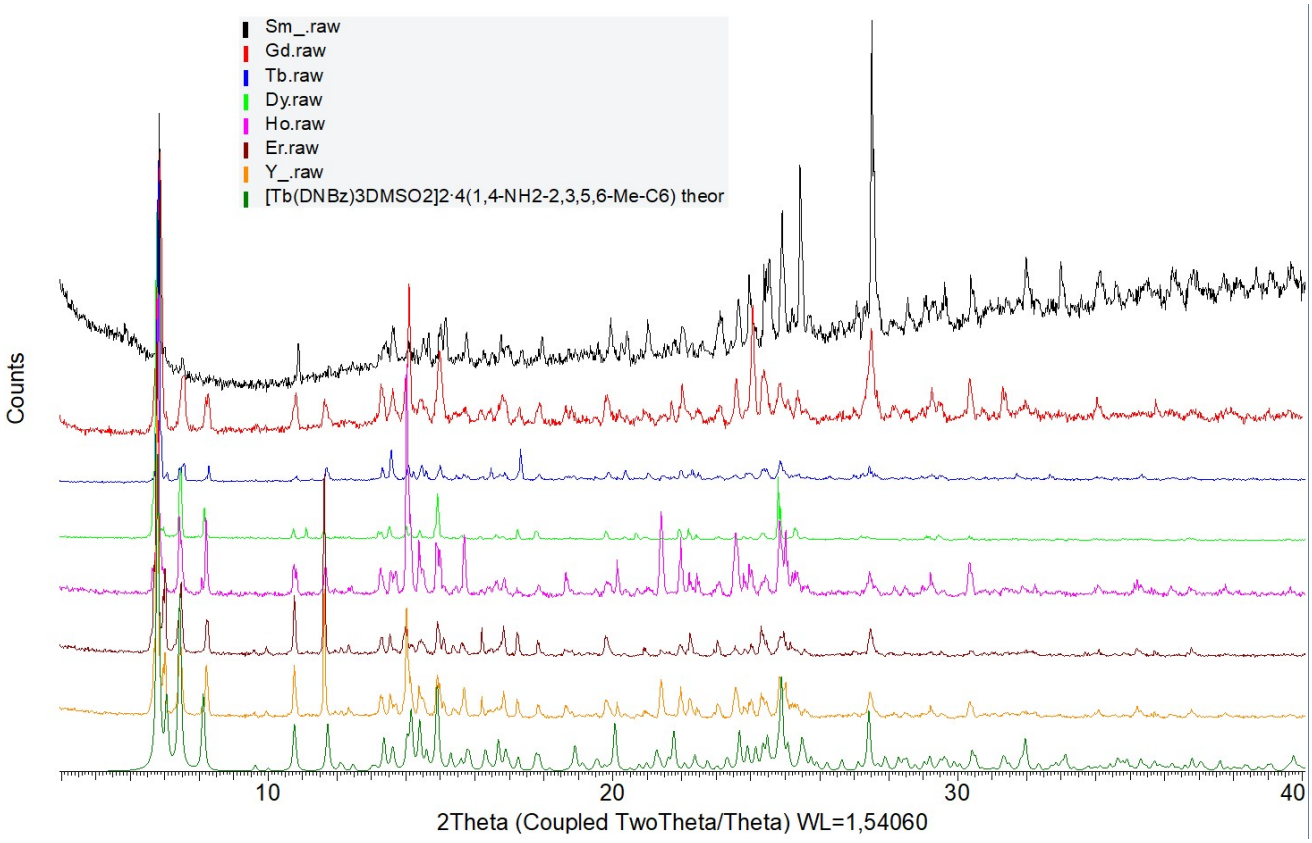

Fig. S18. Powder X-ray diffractograms of the complexes **1**-**7**.